Artificial Pinning Center Nb–Ti Superconductors with Alloyed Nb Pins

Robert W. Heussner, Cristina Bormio Nunes,* Lance D. Cooley and David C. Larbalestier
Applied Superconductivity Center, University of Wisconsin-Madison, WI 53706
*on leave from Faenquil/Demar, 12600-000 Lorena SP, BRAZIL

Abstract—**A magnetic interaction has been proposed as the dominant fluxon-defect interaction in conventional and artificial pinning center (APC) Nb–Ti, emphasizing the proximity length (ξ_N) of the pinning center as the important parameter for optimizing the high field critical current density. We have characterized APC composites containing 25 vol.% of Nb pins alloyed with 7.5 wt.% Ta and 10 wt.% W to deliberately test the predictions of this model. We found that the bulk flux pinning force of the Nb10W-pin composite (ξ_N(Nb10W)~32 nm) exhibited a magnetic field (H) and pin size (d_p) dependency that is more consistent with conventionally processed Nb47Ti (ξ_N(α-Ti)<32 nm) than with existing pure Nb-pin APC composites (ξ_N(Nb)~83 nm). The Nb7Ta-pin composite (ξ_N~59 nm) had intermediate $F_p(H,d_p)$ behavior, thus qualitatively supporting the model.**

I. Introduction

Artificial pinning center (APC) Nb–Ti superconducting wires have demonstrated superior flux pinning properties compared to conventionally processed wires. APC wires with 24 and 28 volume percent of nominally round [1] or planar [2] Nb pins have produced bulk flux pinning forces (F_p) in excess of 30 GN/m^3 at 4.2 K, far surpassing the 18 GN/m^3 [3] achieved in optimized, conventional wires, for which the flux pinning microstructure consists of ~20 vol.% of 1-2 nm thick α-Ti ribbons [4], [5]. However, the reduced magnetic field ($h_{max}=H_{max}/H_{c2}$) at which the maximum in F_p (F_{pmax}) occurs is lower in all existing APC wires. In optimized conventional wire $F_p(H)$ is proportional to h(1-h), giving h_{max}=0.5, while in optimized APC wire with Nb pins, h_{max}~0.25. Although the peak in F_p can be moved to higher reduced fields by decreasing the pin size (thus increasing the pin number density), the magnitude of F_p is also reduced, partly due to an accompanying decrease in H_{c2} [2], [6] caused by the proximity effect. Since many applications demand high critical current density (J_c) at high fields, it is desirable to move F_{pmax} to higher fields in APC wires.

Recently, Cooley et al. [7] proposed that magnetic pinning is the dominant pinning mechanism in both APC and conventional Nb–Ti. In the context of the magnetic pinning model, both F_{pmax} and h_{max} are governed by the pin proximity length (ξ_N), given by

$$\xi_N(T) = \left(\hbar v_F \ell / 6\pi k_B T\right)^{1/2} \quad (1)$$

$$\ell = v_F m / ne^2 \rho \quad (2)$$

where $\hbar$ is the modified Planck constant, v_F is the Fermi velocity, k_B is Boltzmann's constant, ℓ is the electron mean free path, m is the electron rest mass, n is the number of free electrons per unit volume and ρ is the resistivity.

A key prediction of the magnetic pinning model is that the maximum elementary pinning force (f_p) should occur for a pin thickness of ~ξ_N. The maximum bulk pinning force is then the best compromise between getting a high f_p and a high n_p, this condition occurring when the thickness is ~ξ_N/3. Thus, the number density of pins (n_p) at optimum thickness and consequently h_{max}, are determined *solely* by the electronic properties of the pin material. Since ξ_N(α-Ti) is less than ξ_N(Nb), h_{max} is higher for α-Ti pins than for Nb pins. The fact that this is observed experimentally suggests that alloyed Nb pins will exhibit increased values of h_{max}.

In order to test these predictions, we fabricated APC composites with alloyed Nb pins, the aims being (1) to reduce the pin proximity length by shortening the electron mean free path and (2) to use a Nb-rich composition to allow for comparison with already existing APC composites made with pure Nb pins. The second point is particularly important when considering that pins with crystal structures other than the body centered cubic (bcc) structure of Nb can produce markedly different nanostructures. Both Nb 7.5 wt.% Ta (Nb7Ta) and Nb 10 wt.% W (Nb10W) form bcc substitutional solid solutions, exhibit room temperature strain hardening characteristics that are similar to Nb 47 wt.% Ti (Nb47Ti), and have proximity lengths that are significantly shorter, 30% and 60% respectively, than that of pure Nb. Hence, they make good candidates for artificial pins.

II. Experimental Procedure

Pin proximity lengths were calculated from (1) and (2) using the resistivities of 0.23 mm diameter wires measured at 10 K. The pin resistivities were measured in a variable temperature cryostat using a current of 100 mA. Although our values of ξ_N are higher than those established by Cooley et al., we make no attempt in this paper to correct for the simple classical expressions of (1) and (2).

Table I summarizes the fabrication details for the three APC composites, including the number of pins (N_p) and filaments (N_f) and the extrusion temperatures. The Nb-pin APC composite was fabricated using a rod-bundling process

Manuscript received August 27, 1996.
This work was supported in part by the U.S. Department of Energy-Division of High Energy Physics.

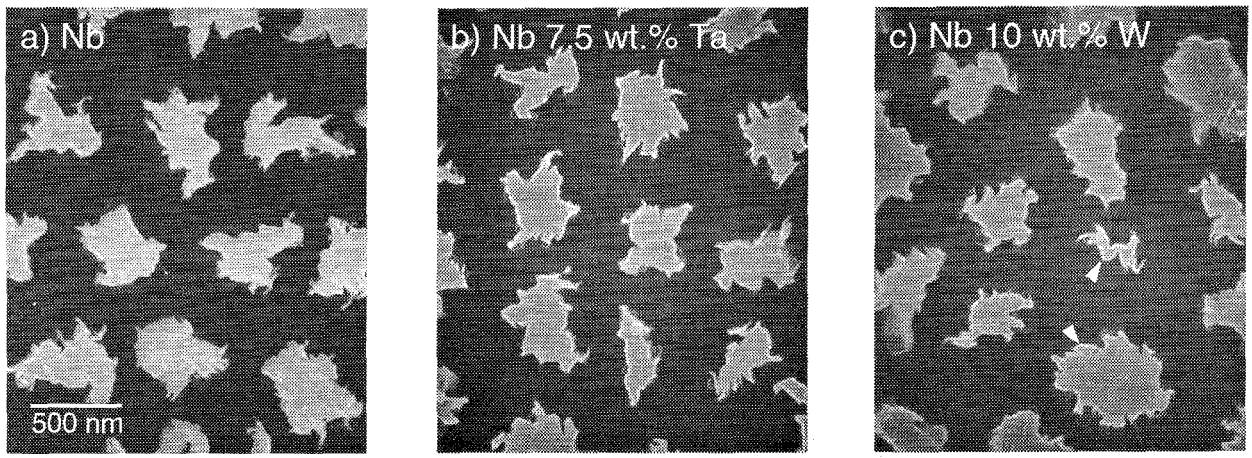

Fig. 1. FESEM secondary-electron images of the a) Nb, b) Nb7Ta and c) Nb10W pinning arrays at a nominal pin diameter of ~400 nm. The wire samples were etched lightly with a mixture of 25% HNO_3, 25% HF and 50% H_2O. Examples of sausaged Nb10W pins are indicated by the arrows in Fig. 1c.

described previously [1], [8]. It contained 24.4 vol.% of pins and produced very high J_c values in fields up to 6 T, including a record J_c(5 T, 4.2 K) of 4600 A/mm^2.

The alloyed Nb-pin APC composites were fabricated by the rod-in-tube method first described in [9], in which a rod of the pin material is inserted into a hole drilled into a rod of Nb–Ti. In our case the pin diameter was 1/2 that of the Nb47Ti rod, thus giving a pin volume fraction of 25%. Each Nb47Ti/alloyed Nb-pin composite was canned in Cu and extruded at ~650°C using an area reduction ratio of 10. The extruded wires were drawn, cut lengthwise into 91 filaments and the Cu was etched off. The filaments were stacked and extruded under the same conditions. The stack and extrusion sequence was followed twice more with 91 and 55 filaments, the final extrusion being made at ~250°C. The Nb7Ta-pin wire was drawn through a hexagonally shaped die at 1.1 mm and 7 filaments were restacked and canned in a Cu tube, the end product being a wire containing 7 superconducting filaments, each filament containing 91×91×55 pinning centers. The Nb10W-pin composite was also designed to be a 7 filament composite, however, during its final extrusion only the front section of the composite billet extruded uniformly and the small portion of good quality wire that resulted had to be drawn down as a monofilament. Each composite was cold drawn to various diameters down to 0.08 mm. Vickers microhardness measurements were made on transverse wire cross sections using 200 g or 1000 g loads applied for 15 s.

Transport critical current (I_c) measurements were made at 4.2 K with the magnetic field applied perpendicular to the wire axis. The voltage tap spacing was 33 cm and a 10^{-14} Ω-m criterion applied over the entire wire cross section was used to determine I_c. J_c was calculated by dividing I_c by the superconductor cross-sectional area. Copper-to-superconductor ratios were determined by weighing, etching the Cu off and reweighing.

III. Results

Table I lists the measured 10 K resistivities and calculated ℓ and ξ_N values for each pin material. The ξ_N values for Nb, Nb7Ta and Nb10W and pure Ti are 83, 59, 32 and 32 nm, respectively.

Figs. 1a, b and c show field emission scanning electron microscope (FESEM) secondary-electron images of the Nb, Nb7Ta and Nb10W composites, respectively, at d_p~400 nm. The nominal pin diameter (d_p) is defined by:

$$d_p = d_w \Big/ \left(N_p / V_f \left(1+R\right)\right)^{1/2} \tag{3}$$

where d_w is the wire diameter, N_p is the number of pins, V_f is the volume fraction of pins and R is the Cu-to-superconductor ratio. In each case, the pin shape was irregular but the

TABLE I
APC Composite Fabrication Details

	Stack No./Extrusion Temp.			
	1/650°C	2/650°C	3/250°C	4/RT[b]
Pin material	N_p	N_f	N_f	N_f
Nb [1]	31	127	55	7
Nb 7.5 wt.% Ta[a]	91	91	55	7
Nb 10 wt.% W[a]	91	91	55	...

[a]These composites were manufactured via the rod-in-tube method [9] and received an extrusion prior to the first restack.
[b]These composites were cold draw stacks.

TABLE II
Artificial Pin Electronic Properties at 10 K

Pin material	ρ_0 (μΩ-cm)	ℓ (nm)	ξ_N (nm)
Nb	0.567	53	83
Nb 7.5 wt.% Ta	1.11	27	59
Nb 10 wt.% W	3.67	7.7	32
Ti	5.61	6.1	32

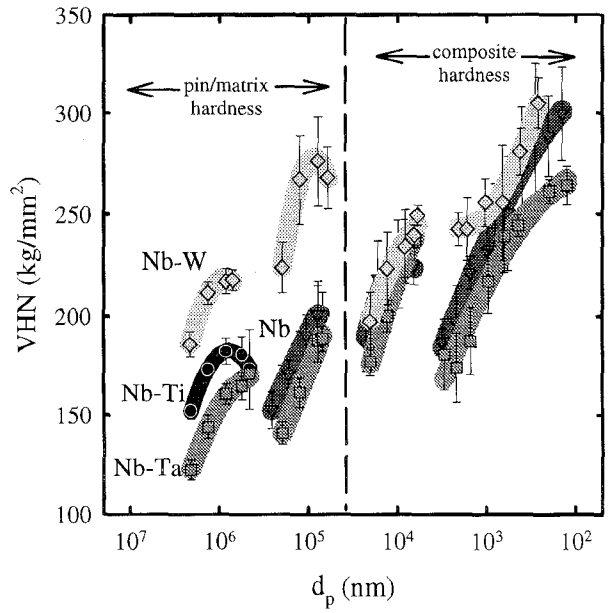

Fig. 2. Vickers microhardness versus nominal pin diameter for the three composites. Data from 5 mm > d_p > 50 μm reflect the pin or Nb–Ti matrix hardness while those from 50 > d_p > 100 nm reflect the overall composite hardness. Breaks between the data sets indicate where the extrusions occurred.

designed hexagonal pin arrangement was still clear. The only noticeable difference between the three pin arrays is that some sausaging of the Nb10W pins occurred, as shown in Fig. 1c. This may be partially the consequence of insufficient work-recrystallization cycles for the Nb10W alloy, which had a different origin from the Nb and Nb7Ta.

Fig. 2 shows the Vickers microhardness as a function of the nominal pin diameter. At larger pin diameters (5 mm > d_p >50 μm), the pin hardness can be determined, but at smaller diameters (50 μm > d_p > 100 nm) only the composite hardness can be measured. Breaks in the data indicate where the warm extrusions occurred. The strain-hardening characteristics of the Nb and Nb7Ta pins and the Nb47Ti matrix are very similar; the hardness increases with cold drawing strain but drops off during extrusion. The Nb10W pins strain harden at a rate similar to the other pins but do not recover during extrusion. As a result, the overall strain hardening rate is higher for both the Nb10W pins and the Nb10W/Nb47Ti composite.

Figs. 3a-c plot the bulk flux pinning force $F_p = J_c \times \mu_0 H$ versus applied field for the Nb, Nb10W and Nb7Ta pin composites, respectively. The development of $F_p(H)$ with decreasing pin diameter shown for the Nb composite in Fig. 3a is similar to that described previously for a composite of identical composition but fabricated using different processing parameters [6]. As the nominal pin diameter drops below 100 nm, a low field peak in $F_p(H)$ emerges, reaching a maximum value of 32 GN/m^3 at 2.5 T for d_p~40 nm. When the pin size is further reduced, the peak position shifts to higher fields, but the magnitude declines. A similar development of $F_p(H, d_p)$ is shown for the Nb7Ta pin composite in Fig. 3b. In this case F_{pmax} reached 25 GN/m^3, but at higher field (3 T) and smaller d_p (35 nm). It should be noted that low field flux jumps in the wires with d_p>35 nm may have prevented measurement of the true F_{pmax}.

The development of $F_p(H)$ over the interval d_p=82-32 nm in the Nb10W-pin composite (Fig. 3c) differs qualitatively from that observed for the pure Nb and Nb7Ta pin composites. It bears a closer resemblance to the development of $F_p(H)$ seen in conventionally processed Nb47Ti [4] during the drawing strain at large pin size, following the last precipitation heat treatment. As in the other APC composites, a low field peak in $F_p(H)$ develops at large d_p, but the optimum curve is not reached, at least until d_p=32 nm (the smallest wire tested). The peak value of F_p, 15 GN/m^3, appears to still be rising with decreasing d_p because there is a comparatively larger increase of F_p with changing d_p at this size than is seen in Figs. 3a and 3b near the optimum value of d_p.

IV. Discussion

As expected, the proximity length of the Nb pins decreased with alloying. The proximity lengths of Nb7Ta (59 nm) and Nb10W (32 nm) are 30% and 60% shorter, respectively, than that of pure Nb (83 nm). Nb10W has the same ξ_N as that measured for pure Ti [10], but ξ_N for α-Ti is likely even shorter because it is alloyed with 5 at.% Nb [5].

The trends seen in the $F_p(H,d_p)$ curves of Fig. 3 are qualitatively consistent with the magnetic pinning model. As the pin proximity length was reduced, the value of h_{max} increased and F_{pmax} occurred at smaller nominal pin diameters. Stronger validation of the magnetic pinning model may come with the identification of h_{max} and F_{pmax} in the Nb10W-pin composite, which unfortunately, was not possible in this experiment due to the fabrication difficulties discussed above.

APC fabrication improvements are still being made. Our recent work on pure Nb pin APC composites [1] produced large increases (~40%) in F_{pmax} with little change in h_{max}. Nb 7.5 wt.% Ta seems almost identical to Nb in hardness, work-hardening and fabricability. However, the Nb10W was markedly worse, undoubtedly because W has a smaller atomic radius (0.142 nm) than both Nb and Ta (0.147 nm), causing the increased work-hardening shown in Fig. 2. However, the 32 nm limit placed on the Nb10W pin size in this experiment should not be considered as a severe obstacle to fabricating wires with smaller nominal pin size. Composite break-up during the final extrusion may have been more a result of the billet design and extrusion parameters not being optimized for the higher overall Nb47Ti/Nb10W composite hardness, rather than as a direct consequence of the pin/matrix hardness disparity. This hypothesis is supported by the fact that the Nb10W pin composite drew well following the final extrusion; the pin sausaging seen in Fig. 1c did not adversely

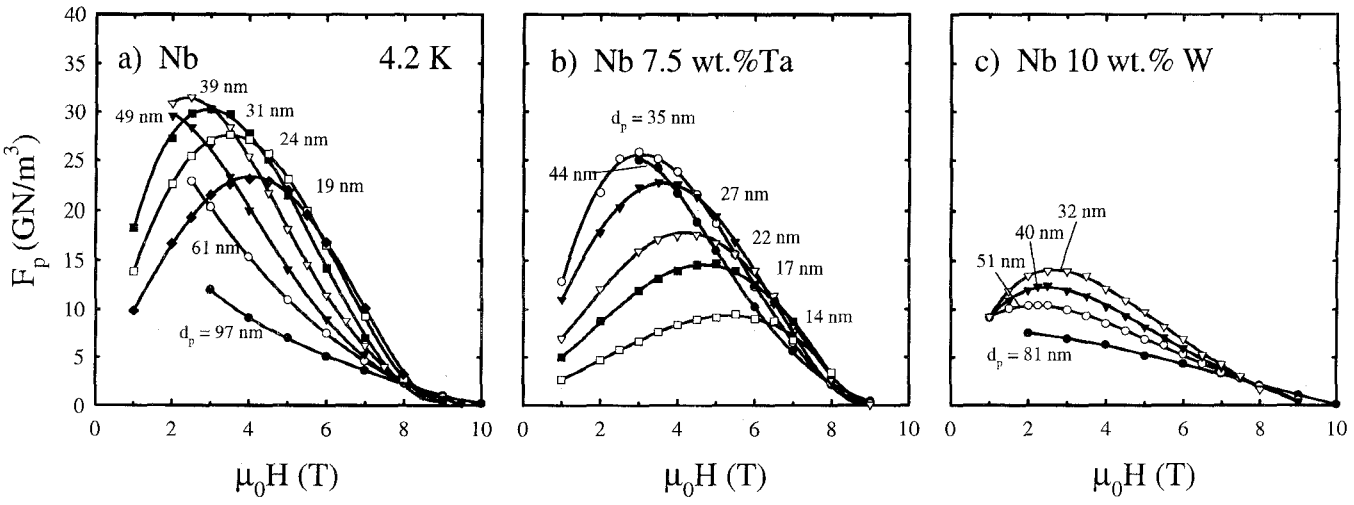

Fig. 3. Bulk flux pinning force versus applied field for the a) Nb, b) Nb7Ta and c) Nb10W-pin APC composites at 4.2 K. Note that wires with $d_p < 32$ nm were not fabricated for the Nb10W-pin composite due to fabrication difficulties.

affect its drawability. Future experiments will investigate Nb10W-pin APC wires in more detail, especially in the lower limit of d_p.

V. Conclusions

APC Nb 47 wt.% Ti wires containing 25 vol.% of alloyed Nb pins were fabricated to evaluate the effect of the pin proximity length ξ_N on the flux pinning properties. The proximity length of pure Nb, 83 nm, decreased to 59 nm and 32 nm when alloyed with 7.5 wt.% Ta and 10 wt.% W, respectively. The field and pin thickness dependence of the F_p curves qualitatively support the magnetic pinning model; as ξ_N decreased, the field and pin thickness at which the maximum F_p occurred increased and decreased, respectively. Excessive hardening of the Nb10W-pin composite, an adverse effect of the tungsten alloying addition, caused composite fabrication difficulties and prevented wires with d_p<32 nm from being fabricated. Future work will investigate the role of ξ_N in greater detail.

Acknowledgments

We gratefully acknowledge P. Lee, A. Gurevich, E. Kadyrov, W. Starch, A. Squitieri, M. Pelletier, M. Schlinkert and A. Lindner for discussions and experimental assistance and P. Jablonski and P. Morris with Teledyne Wah Chang for donating the Nb–Ti and Nb7Ta rods. The scanning electron microscopy was partially supported through the Integrated Microscopy Resource, Madison, WI which is supported through a NIH Biomedical Research Technology Grant.

References

[1] R.W. Heussner, J.D. Marquardt, P.J. Lee and D.C. Larbalestier, to appear Appl. Phys. Lett., 1997.
[2] K. Matsumoto, H. Takewaki, Y. Tanaka, O. Miura, K. Yamafuji, K. Funaki, M. Iwakuma and T. Matsushita, Appl. Phys. Lett., vol. 64, 1994, pp. 115-117.
[3] C. Li and D.C. Larbalestier, Cryogenics, vol. 27, 1987, pp. 171-177.
[4] C. Meingast, P.J. Lee and D.C. Larbalestier, J. Appl. Phys., vol. 66, 1989, pp. 5962-5970.
[5] P. J. Lee and D.C. Larbalestier, Acta. Metall, vol. 35, 1987, pp. 2526-2536.
[6] R.W. Heussner, C.B. Nunes, P.J. Lee, D.C. Larbalestier and P.D. Jablonski, J. Appl. Phys., vol. 80, 1996, pp. 1640-1646.
[7] L.D. Cooley, P.J. Lee and D.C. Larbalestier, Phys. Rev. B, vol. 53, 1996, pp. 6638-6652.
[8] R.W. Heussner, P.D. Jablonski, P.J. Lee and D.C. Larbalestier, IEEE Trans. Appl. Supercond., vol. 5, 1995, pp. 1705-1708.
[9] B. A. Zeitlin, M.S. Walker and L. R. Motowidlo, United States Patent No. 4,803,310 (Feb 7, 1989).
[10] C.B. Nunes, unpublished work.